



DIGITAL ACCESS TO SCHOLARSHIP AT HARVARD

Estradiol promotes pentose phosphate pathway addiction and cell survival via reactivation of Akt in mTORC1 hyperactive cells

The Harvard community has made this article openly available. [Please share](#) how this access benefits you. Your story matters.

Citation	Sun, Y., X. Gu, E. Zhang, M. Park, A. M. Pereira, S. Wang, T. Morrison, et al. 2014. "Estradiol promotes pentose phosphate pathway addiction and cell survival via reactivation of Akt in mTORC1 hyperactive cells." Cell Death & Disease 5 (5): e1231. doi:10.1038/cddis.2014.204. http://dx.doi.org/10.1038/cddis.2014.204 .
Published Version	doi:10.1038/cddis.2014.204
Accessed	February 16, 2015 10:57:35 AM EST
Citable Link	http://nrs.harvard.edu/urn-3:HUL.InstRepos:12406657
Terms of Use	This article was downloaded from Harvard University's DASH repository, and is made available under the terms and conditions applicable to Other Posted Material, as set forth at http://nrs.harvard.edu/urn-3:HUL.InstRepos:dash.current.terms-of-use#LAA

(Article begins on next page)

Estradiol promotes pentose phosphate pathway addiction and cell survival via reactivation of Akt in mTORC1 hyperactive cells

Y Sun¹, X Gu², E Zhang¹, M-A Park¹, AM Pereira¹, S Wang¹, T Morrison¹, C Li¹, J Blenis², VH Gerbaudo¹, EP Henske¹ and JJ Yu^{*1}

Lymphangioleiomyomatosis (LAM) is a female-predominant interstitial lung disease that can lead to respiratory failure. LAM cells typically have inactivating *TSC2* mutations, leading to mTORC1 activation. The gender specificity of LAM suggests that estradiol contributes to disease development, yet the underlying pathogenic mechanisms are not completely understood. Using metabolomic profiling, we identified an estradiol-enhanced pentose phosphate pathway signature in *Tsc2*-deficient cells. Estradiol increased levels of cellular NADPH, decreased levels of reactive oxygen species, and enhanced cell survival under oxidative stress. Mechanistically, estradiol reactivated Akt in *TSC2*-deficient cells *in vitro* and *in vivo*, induced membrane translocation of glucose transporters (GLUT1 or GLUT4), and increased glucose uptake in an Akt-dependent manner. ¹⁸F-FDG-PET imaging demonstrated enhanced glucose uptake in xenograft tumors of *Tsc2*-deficient cells from estradiol-treated mice. Expression array study identified estradiol-enhanced transcript levels of glucose-6-phosphate dehydrogenase (G6PD), the rate-limiting enzyme of the pentose phosphate pathway. Consistent with this, G6PD was abundant in xenograft tumors and lung metastatic lesions of *Tsc2*-deficient cells from estradiol-treated mice. Molecular depletion of G6PD attenuated estradiol-enhanced survival *in vitro*, and treatment with 6-aminonicotinamide, a competitive inhibitor of G6PD, reduced lung colonization of *Tsc2*-deficient cells. Collectively, these data indicate that estradiol promotes glucose metabolism in mTORC1 hyperactive cells through the pentose phosphate pathway via Akt reactivation and G6PD upregulation, thereby enhancing cell survival under oxidative stress. Interestingly, a strong correlation between estrogen exposure and G6PD was also found in breast cancer cells. Targeting the pentose phosphate pathway may have therapeutic benefit for LAM and possibly other hormonally dependent neoplasms.

Cell Death and Disease (2014) 5, e1231; doi:10.1038/cddis.2014.204; published online 15 May 2014

Subject Category: Cancer Metabolism

Lymphangioleiomyomatosis (LAM), a rare cystic lung disease with multi-organ involvement, occurs primarily in women of childbearing age.^{1–3} LAM is characterized pathologically by widespread proliferation of abnormal smooth muscle cells and by cystic changes within the lung parenchyma.^{1–3} About 60% of women with the sporadic form of LAM also have renal angiomyolipomas. The presence of *TSC2* mutations in LAM cells and renal angiomyolipoma cells from women with sporadic LAM, but not in normal tissues, has led to the hypothesis that LAM cells spread to the lungs via a metastatic mechanism,⁴ despite the fact that LAM cells have a histologically benign appearance. Genetic and fluorescent *in situ* hybridization analyses of recurrent LAM after lung transplantation support this benign metastatic model.^{4,5}

Alterations in cellular energy metabolism are a hallmark of cancer.⁶ Many cancer cells generate the majority of their ATP

by converting glucose to lactate, a process that was first recognized in 1930 and is referred to as the Warburg effect.⁷ There are several indications that cells carrying mutations in the *TSC* genes have defects in energy metabolism. Cells lacking *TSC2* undergo massive apoptosis in glucose-free growth conditions.⁸ Rapamycin reduces lactate production but does not affect cellular ATP levels in *Tsc2*^{-/-} MEF cells.⁹ Cells lacking *Tsc1* or *Tsc2* have increased expression of genes encoding the enzymes of lipid and sterol biosynthesis, glycolysis, and the pentose phosphate pathway.¹⁰ Cells with mTOR hyperactivation exhibit PKM2-stimulated glycolysis.¹¹ Pentose phosphate pathway is a critical autophagy-dependent compensatory metabolic reprogramming in *Tsc2*-deficient cells.¹² Despite these findings, the role of estradiol in regulating cellular metabolism in *Tsc2*-deficient cells has not been extensively investigated.

¹Division of Pulmonary and Critical Care Medicine, Department of Medicine, Brigham and Women's Hospital and Harvard Medical School, 1 Blackfan Circle, 6th Floor, Boston, MA 02115, USA and ²Department of Cell Biology, Harvard Medical School, Boston, MA 02115, USA

*Corresponding author: JJ Yu, Division of Pulmonary and Critical Care Medicine, Brigham and Women's Hospital, Harvard Medical School, 1 Blackfan Circle, 6th Floor, Boston, MA 02115, USA. Tel: +1 617 355 9018; Fax: +1 617 355 9016; E-mail: jyu13@rics.bwh.harvard.edu

Keywords: tuberlin; Akt; pentose phosphate pathway; glucose transporters; glucose uptake; 6-aminonicotinamide

Abbreviations: 6-AN, 6-aminonicotinamide; ¹⁸F-FDG-PET, fluodeoxyglucose positron emission tomography; ATP, adenosine triphosphate; E₂, 17β-estradiol; ER, estrogen receptor; ERK, extracellular signal-regulated kinases; G6PD, glucose-6-phosphate dehydrogenase; GLUT1/4, glucose transporter1/4; H₂O₂, hydrogen peroxide; LAM, lymphangioleiomyomatosis; mTORC1, mammalian target of rapamycin complex 1; MEF, mouse embryonic fibroblasts; NADPH, nicotinamide adenine dinucleotide phosphate; PKM2, pyruvate kinase muscle isozyme 2; SCID, severe combined immunodeficiency; TBC1D7, TBC1 domain family member 7; TCGA, The Cancer Genome Atlas; TSC2, tuberous sclerosis complex 2

Received 11.1.14; revised 26.3.14; accepted 08.4.14; Edited by C Munoz-Pinedo

The female predominance of LAM, coupled with the genetic data indicating that LAM cells are metastatic, suggests that estradiol may promote the metastasis of Tsc2-deficient cells. Both LAM cells and angiomyolipoma cells express estradiol receptor alpha and progesterone receptor, and the symptoms of LAM can worsen during pregnancy.^{1–3} Although we have previously found that estradiol promotes the survival and metastasis of Tsc2-deficient cells, the molecular and cellular mechanisms that may underlie this are not completely understood.

We report here that estradiol treatment of TSC2-deficient cells is associated with elevated levels of pentose phosphate pathway intermediates, Akt-dependent membrane translocation of the glucose transporters (GLUT1 or GLUT4), and enhanced glucose uptake *in vitro* and *in vivo*. 6-amino-nicotinamide (6-AN), a competitive inhibitor of the pentose phosphate pathway,¹³ suppressed estradiol-induced cell survival *in vitro* and *in vivo*. Taken together, these data reveal that pentose phosphate pathway is a critical component of the estradiol-dependent cell survival of TSC2-deficient cells, and point toward novel therapeutic targets for LAM and potentially for other hormonally dependent neoplasms associated with mTORC1 activation.

Results

Identification of estradiol-induced metabolic signature of the pentose phosphate pathway in Tsc2-deficient cells.

To elucidate pro-survival events mediated by estradiol (E_2) in Tsc2-deficient rat uterus-derived ELT3 cells,^{14,15} we performed a metabolomics screen by LC/MS/MS. A significant increase in glycolysis and pentose phosphate pathway intermediates (Figure 1a), including glucose (3.6-fold), glucose-6-phosphate (2.6-fold), fructose-6-phosphate (2.5-fold), ribose (3.6-fold), ribose-5-phosphate (2.2-fold), and ribulose-5-phosphate (2.2-fold), were observed in E_2 -stimulated cells at 24 h (Figure 1b). Furthermore, E_2 increased the cellular levels of NADPH (Figure 1c) and decreased the levels of reactive oxygen species (ROS) (Figure 1d) in the presence or absence of hydrogen peroxide (H_2O_2) at 24 h. However, E_2 did not affect the secretion of lactate, the end product of glycolysis (Figure 1e).

To determine the effect of E_2 in the survival of TSC2-deficient cells under oxidative stress, cells were treated with

H_2O_2 or vehicle for 0.5 h in the presence or absence of E_2 for additional 24 h. H_2O_2 -triggered cell death was strongly rescued by E_2 stimulation by 26% ($P < 0.01$) in comparison with vehicle control in LAM patient-derived cells (Figures 1f and g). Using the PI exclusion assay, E_2 significantly reduced H_2O_2 -induced cell death by 50% ($P < 0.01$) relative to control in rat-derived cells (Figures 1h and i). These data suggest that E_2 enhances the survival of ELT3 cells particularly under conditions of oxidative stress. Collectively, these data indicate that E_2 promotes pentose phosphate pathway addiction in cells lacking TSC2 (Figure 1j).

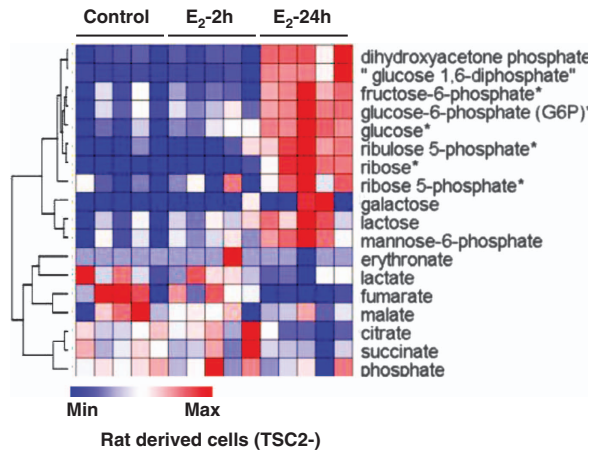
Estradiol reactivates Akt in TSC2-deficient cells *in vitro* and *in vivo*.

To define signaling events that potentially mediate E_2 -enhanced glucose metabolism, we examined the activation of Akt and ERK1/2, which are known signaling molecules influenced by E_2 . Under basal conditions, levels of phospho-Akt S473 were lower in TSC2-deficient LAM patient-derived cells relative to TSC2-addback cells (Figure 2a), as expected. Interestingly, E_2 strongly reactivates Akt (S473) at 1 h and sustains Akt activation to 24 h in TSC2-deficient LAM patient-derived cells (TSC2–) (Figure 2b). We also found that E_2 activates ERK1/2 (T202/Y204), as expected. In contrast, E_2 modestly stimulates Akt at 1 h to 8 h in TSC2-re-expressing cells (TSC2+) (Figure 2c). Notably, E_2 did not further enhance phosphorylation of ribosomal protein S6 (S6) (S235/236) (Figures 2b and c). Next, we examined Akt activation in Tsc2-deficient ELT3 cells, and found that E_2 stimulation resulted in a biphasic activation of Akt at 15–30 min and 6 h *in vitro* (Figure 2d). E_2 also induced a biphasic activation of ERK1/2, as previously reported.^{16–18}

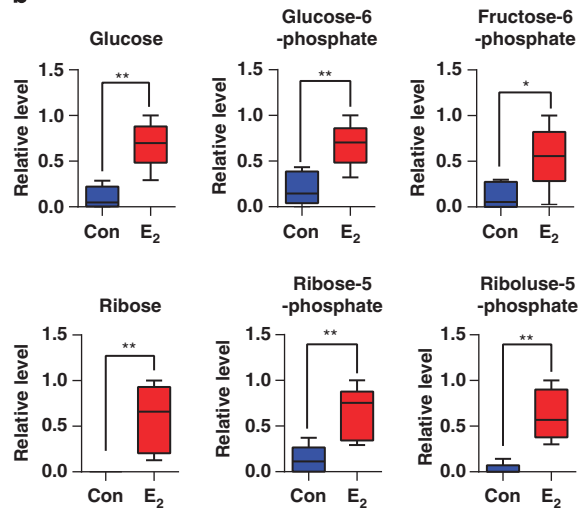
To assess the effect of E_2 in Akt activation *in vivo*, we subcutaneously inoculated ELT3 cells into ovariectomized female SCID mice supplemented with E_2 or placebo. E_2 treatment led to a 2.3-fold increase of tumor volume at 8 weeks post cell inoculation (Figure 2e). Immunoblotting analysis showed that xenograft tumors from E_2 -treated mice have higher levels of phospho-Akt (S473) and phospho-ERK (T202/Y204) compared with placebo treatment (Figure 2f). Moreover, immunohistochemical staining showed that xenograft tumors from E_2 -treated mice exhibit higher levels of phospho-Akt (Ser473) relative to the placebo treatment (Figure 2g). Because Tsc2-deficient cells exhibit low Akt

Figure 1 Identification of estradiol-induced metabolic signature of pentose phosphate pathway in Tsc2-deficient cells *in vitro*. (a) ELT3 (Tsc2-deficient rat uterus-derived) cells were treated with estradiol (10 nM) for 2 and 24 h. Cellular metabolites were profiled by mass spectrometry ($n = 5$) (Metabolon LC-MS/MS). (b) Box-plots of glucose, glucose-6-phosphate, fructose-6-phosphate, ribose, ribose-5-phosphate, and ribulose-5-phosphate are shown. Data show the mean of five sets of independent samples. (c) Cellular NADPH levels were measured in rat-derived Tsc2-deficient cells treated with control or estradiol (10 nM) for 2 and 24 h. Data were normalized to total protein level. Results are representative of three sets of independent samples per group from three experiments. (d) Cellular ROS levels were measured using DCFH-DA in rat-derived Tsc2-deficient cells treated with control or estradiol (10 nM) for 24 h. Cells were incubated with hydrogen peroxide (H_2O_2) (0.5 μ M) for 1 h before measurement. Data were normalized to total cell number. Results are representative of eight independent samples per group from three experiments. (e) Extracellular lactate levels were measured in rat-derived Tsc2-deficient cells treated with control or estradiol (10 nM) for 24 h. FBS (10%) stimulation was included as a positive control. Lactate levels were normalized to total proteins. Results are representative of three sets of independent samples per group from three experiments. (f) Patient-derived TSC2-deficient cells were treated with control or estradiol (10 nM) for 24 h, and then incubated with hydrogen peroxide (0.5 μ M) for 0.5 h. Cell morphology was recorded using phase-contrast microscopy. (g) Patient-derived TSC2-deficient cells were treated with control or estradiol (10 nM) for 24 h, and then incubated with H_2O_2 (0.5 μ M) for 0.5 h. Cell death was measured using the propidium iodide (PI) exclusion assay. Proportion of dead cells was normalized to the total number of variable cells. Results are representative of eight independent samples per group from three experiments. (h) Rat-derived Tsc2-deficient cells were treated with control or estradiol (10 nM) for 24 h, and then incubated with hydrogen peroxide (0.5 μ M) for 1 h. Cell morphology was recorded using phase-contrast microscopy. (i) Rat-derived Tsc2-deficient cells were treated with control or estradiol (10 nM) for 24 h, and then incubated with H_2O_2 (0.5 μ M) for 1 h. Cell death was measured using the PI exclusion assay. Proportion of dead cells was normalized to the total number of variable cells. Results are representative of eight independent samples per group from three experiments. (j) Scheme of glucose metabolism in TSC2-deficient cells treated with estradiol. * $P < 0.05$, ** $P < 0.01$

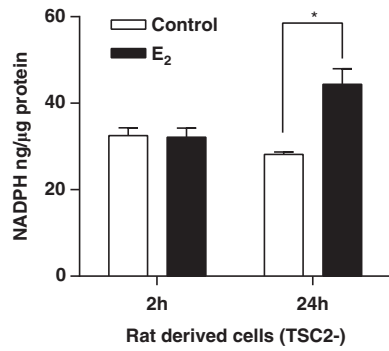
a



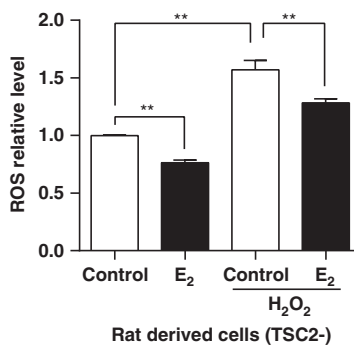
b



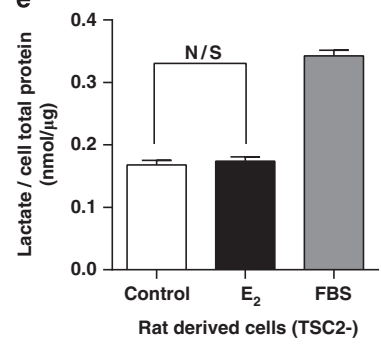
c



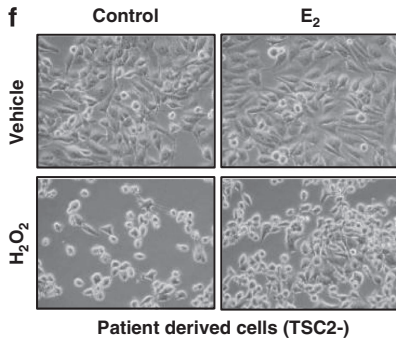
d



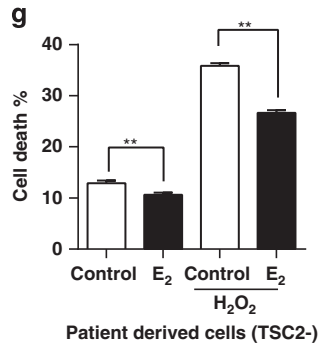
e



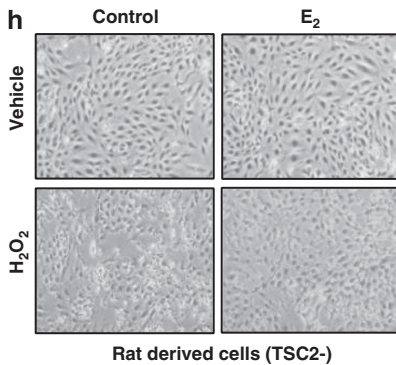
f



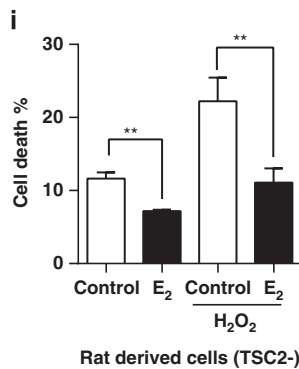
g



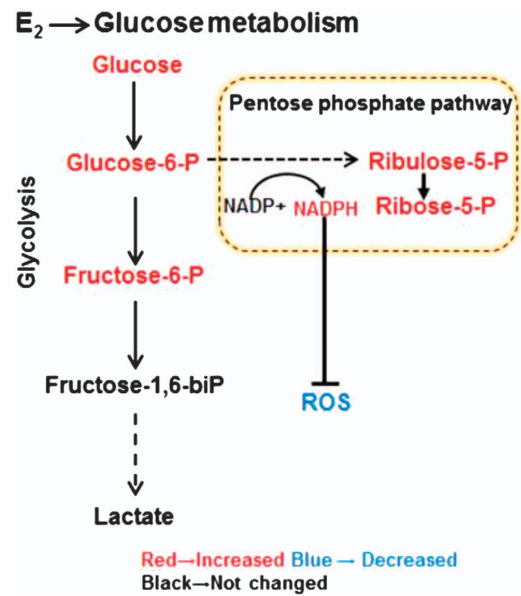
h



i



j



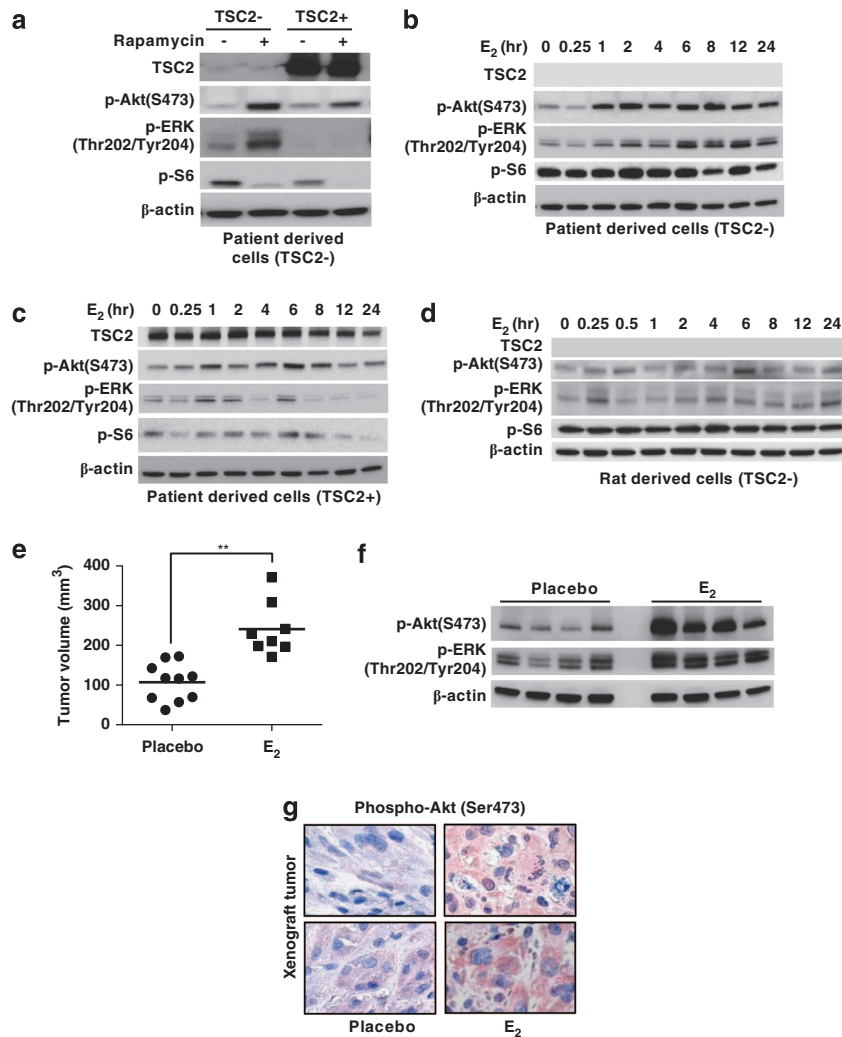


Figure 2 Estradiol reactivates the Akt signaling pathway *in vitro* and *in vivo*. (a) Immunoblot analyses of TSC2, phospho-Akt (Ser473), phospho-ERK1/2 (Thr202/Tyr204), phospho-S6 (Ser235/236), and β -actin in patient-derived TSC2-deficient or TSC2-re-expressing cells treated with control or rapamycin for 12 h. Results are representative of three independent experiments. (b and c) Immunoblot analyses of TSC2, phospho-Akt (S473), phospho-ERK (Thr202/Tyr204), phospho-S6 (Ser235/236), and β -actin in patient-derived TSC2-deficient or TSC2-re-expressing cells treated with estradiol. Results are representative of three different experiments. (d) Immunoblot analyses of TSC2, phospho-Akt (S473), phospho-ERK (Thr202/Tyr204), phospho-S6 (Ser235/236), and β -actin in rat-derived Tsc2-deficient cells treated with estradiol. Results are representative of three different experiments. (e) ELT3 cells were subcutaneously injected into female ovariectomized mice implanted with estradiol or placebo pellets. Tumor volume was calculated at week 8 post cell inoculation. (f) Immunoblot analyses of phospho-Akt (S473), phospho-ERK (Thr202/Tyr204), and β -actin in xenograft tumors from mice treated with estradiol or placebo. (g) Immunohistochemistry of phospho-Akt (Ser473) in xenograft tumors of rat-derived Tsc2-deficient cells from mice treated with estradiol or placebo. Results are representative of five mice in each group. ** $P < 0.01$

activation due to feedback inhibition mechanism,¹⁹ these data reveal that E_2 reactivates Akt pathway in cells lacking TSC2.

Estradiol promotes plasma membrane translocation of glucose transporters GLUT1 or GLUT4 and glucose uptake in an Akt-dependent manner. Glucose entry into cells is facilitated by proper localization of glucose transporters including GLUT1 and GLUT4.²⁰ To examine the impact of E_2 on GLUT1 and GLUT4 localization, TSC2-deficient LAM patient-derived or rat-derived cells were treated with E_2 for 24 h. Confocal microscopy showed that E_2 promoted plasma membrane translocation of GLUT4, but not GLUT1, compared with control in LAM patient-derived cells (Figure 3a). Interestingly, treatment of mTORC1 inhibitor rapamycin led to plasma membrane translocation of GLUT4.

Importantly, E_2 -promoted membrane localization of GLUT4 was abolished by wortmannin treatment (Figure 3a). Furthermore, Akt inhibitors MK2206 and wortmannin strongly suppressed E_2 -induced phosphorylation of Akt (S473), but not phosphorylation of ERK or S6, in patient-derived cells (Figure 3b). Moreover, analysis of rat-derived Tsc2-deficient cells showed that rapamycin treatment led to plasma membrane localization of GLUT1 (Figure 3c). Importantly, E_2 promoted membrane localization of GLUT1, which was abolished by wortmannin treatment (Figure 3c). Immunoblot analysis showed that wortmannin treatment markedly decreased E_2 -induced phosphorylation of Akt (S473), but not phosphorylation of S6 (Figure 3d). Together, these data suggest that Akt specifically mediates the effect of E_2 on GLUT1 or GLUT4 trafficking in TSC2-deficient cells.

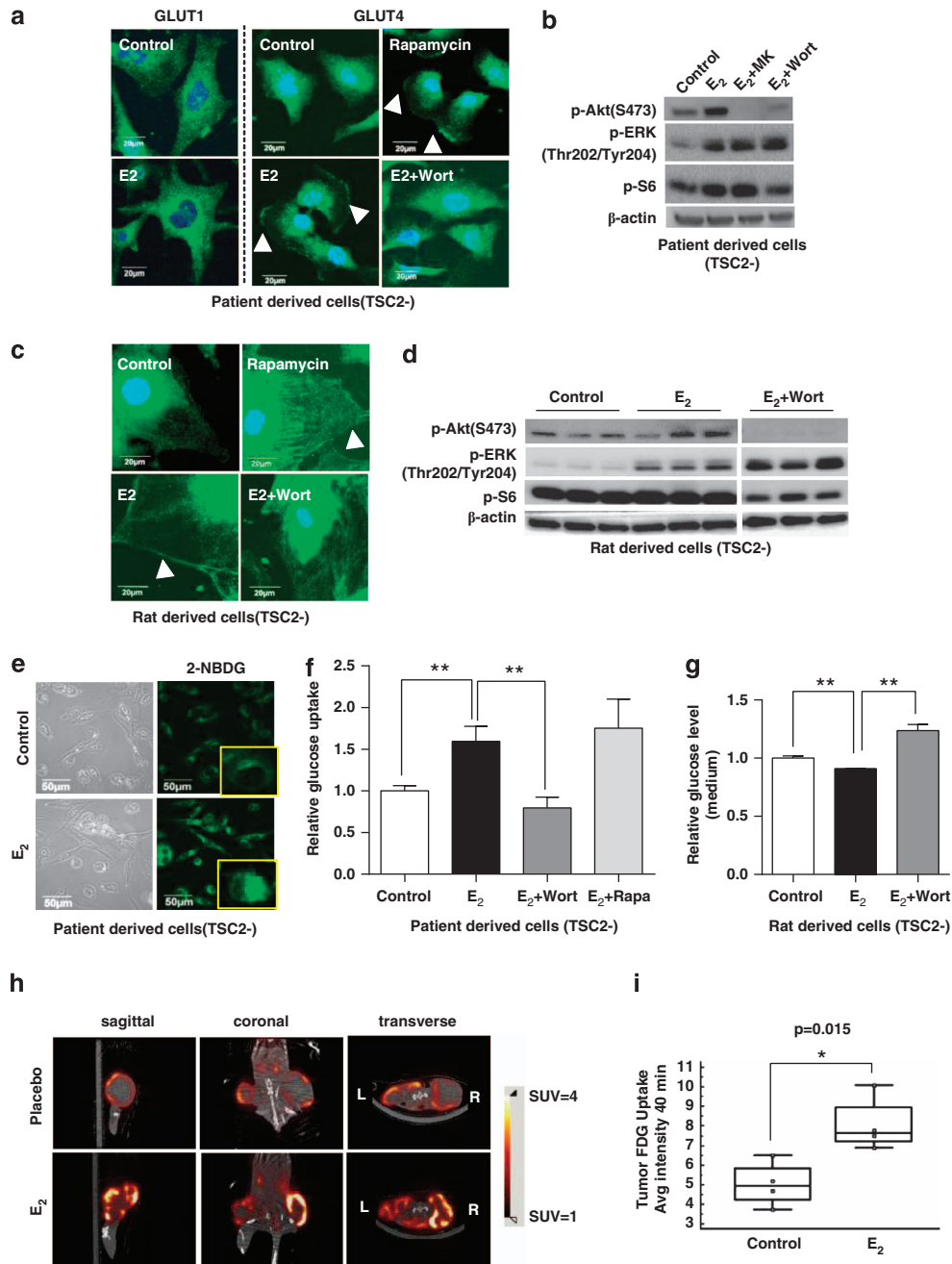


Figure 3 Estradiol enhances GLUT1 and GLUT4 plasma membrane translocation and glucose uptake via PI3K/Akt in TSC2-deficient cells. (a) Patient-derived Tsc2-deficient cells were treated with rapamycin (10 nM), wortmannin (500 nM) for 15 min, and then treated with control or estradiol (10 nM) for 12 h. Subcellular localization of GLUT1 and GLUT4 was examined using confocal microscopy. (b) Patient-derived Tsc2-deficient cells treated with estradiol (10 nM) at 12 h in the presence or absence of MK2206 (2 μ M) or wortmannin (500 nM) for 15 min. Immunoblot analyses of phospho-Akt (Ser473), phospho-ERK1/2 (Thr202/Tyr204), phospho-S6 (Ser235/236), and β -actin. Results are representative of three independent experiments. (c) Rat-derived Tsc2-deficient cells were treated with rapamycin (10 nM), or wortmannin (1 μ M) for 15 min, and then treated with control or estradiol (10 nM) for 24 h. Subcellular localization of GLUT1 was examined using confocal microscopy. (d) Patient-derived TSC2-deficient cells treated with estradiol (10 nM) at 12 h in the presence or absence of wortmannin (500 nM) for 15 min. Immunoblot analyses of phospho-Akt (Ser473), phospho-ERK1/2 (Thr202/Tyr204), phospho-S6 (Ser235/236), and β -actin. Results are representative of three independent experiments. (e) 2-NBDG uptake was measured in patient-derived cells treated with control or estradiol. (f) Glucose uptake was measured by 2-NBDG fluorescence in patient-derived TSC2-deficient cells treated with estradiol in the presence or absence of wortmannin (500 nM) or rapamycin (10 nM) for 15 min before treatment. (g) Rat-derived Tsc2-deficient cells were treated with wortmannin (500 nM) for 15 min, and then treated with control or estradiol (10 nM) for 24 h. Extracellular glucose levels were measured in conditioned media. Data were normalized to the control group. (h) Representative images of [¹⁸F]FDG-PET/CT scanning of estradiol or placebo-treated mice bearing xenograft tumors of ELT3 cells. (i) The graph indicates the average intensity at 40 min of tumor FDG uptake. * $P < 0.05$, ** $P < 0.01$

To determine the impact of E₂ on glucose uptake *in vitro*, we first assessed the direct glucose uptake using 2-NBDG (2-(N-(7-nitrobenz-2-oxa-1,3-diazol-4-yl)amino)-2-deoxyglucose), a fluorescently labeled deoxyglucose analog. Confocal microscopy showed that E₂ treatment led to higher levels of internalized 2-NBDG relative to vehicle treatment (Figure 3e). Fluorescent quantification showed that E₂ treatment increased 2-NBDG uptake by 60% ($P < 0.01$) at 30 min compared with vehicle treatment (Figure 3f), and this was significantly decreased by wortmannin treatment ($P < 0.01$,

but not affected by rapamycin treatment in patient-derived cells (Figure 3f). We next examined the rate of glucose consumption in conditioned media. E₂ significantly increased glucose consumption by ~10% ($P < 0.01$) in comparison with vehicle at 24 h (Figure 3g), indicating that E₂ enhanced glucose uptake in rat-derived Tsc2-deficient ELT3 cells. Importantly, wortmannin treatment reduced the rate of E₂-enhanced glucose uptake (Figure 3g). Collectively, these data demonstrate that Akt specifically mediates the effect of E₂ on glucose uptake in cells lacking TSC2 *in vitro*.

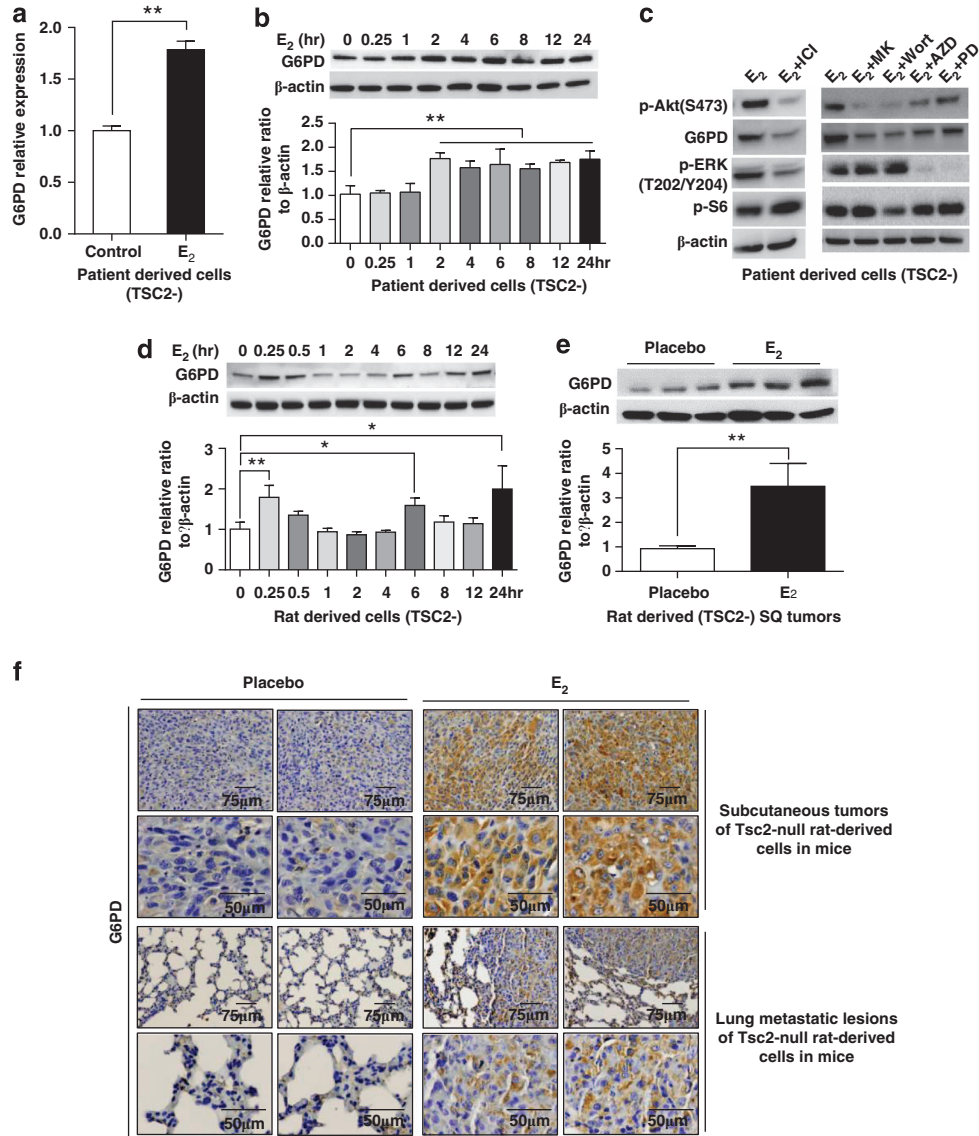


Figure 4 G6PD expression is elevated in Tsc2-deficient cells *in vitro* and *in vivo*. (a) Transcript levels of G6PD were measured using real-time RT-PCR in patient-derived TSC2-deficient cells treated with control or estradiol. (b) Immunoblot analyses of G6PD and β -actin in patient-derived TSC2-deficient cells treated with estradiol. A densitometry analysis of G6PD was performed. Results are representative of three different experiments. (c) Immunoblot analyses of phospho-Akt (Ser473), G6PD, phospho-ERK1/2 (Thr202/Tyr204), phospho-S6 (Ser235/236), and β -actin in patient-derived TSC2-deficient cells treated with estradiol for 12 h in the presence or absence of MK2206 (2 μ M), wortmannin (500 nM), AZD6244 (500 nM), or PD98059 (50 μ M) for 15 min before treatment. Results are representative of three different experiments. (d) Immunoblot analyses of G6PD and β -actin in rat-derived Tsc2-deficient cells treated with estradiol at the indicated time points. A densitometry analysis of G6PD was performed. Results are representative of three different experiments. (e) Immunoblot analyses levels of G6PD and β -actin in xenograft tumors of ELT3 cells. A densitometry analysis of G6PD was performed. Results are representative of three different experiments. (f) Immunohistochemistry of G6PD in xenograft tumors of ELT3 cells and lung metastatic lesions from mice treated with estradiol or placebo. Results are representative of five mice in each group. * $P < 0.05$, ** $P < 0.01$

To determine whether E₂ affects glucose uptake *in vivo*, E₂ or placebo-treated mice bearing established xenograft tumors of Tsc2-deficient ELT3 cells were subjected to 2-[¹⁸F]Fluoro-2-deoxyglucose positron emission tomography/computed tomography (FDG-PET/CT) imaging. The representative images show the [¹⁸F]FDG-PET/CT scanning of E₂ or placebo-treated mice bearing xenograft tumors of ELT3 cells

(Figure 3h). The FDG uptake in the tumors on the left for both mice appeared to be similar. However, standardized uptake value (SUV)_{max} measured over the volume of the tumor indicated a higher FDG uptake in E₂ (SUV_{max} = 7.54 (right) and 6.88 (left)) than in the control animal (SUV_{max} = 4.72 (right) and 3.74 (left)) (Figure 3i). The average tumor FDG uptake increased by ~50% in E₂-treated mice relative to

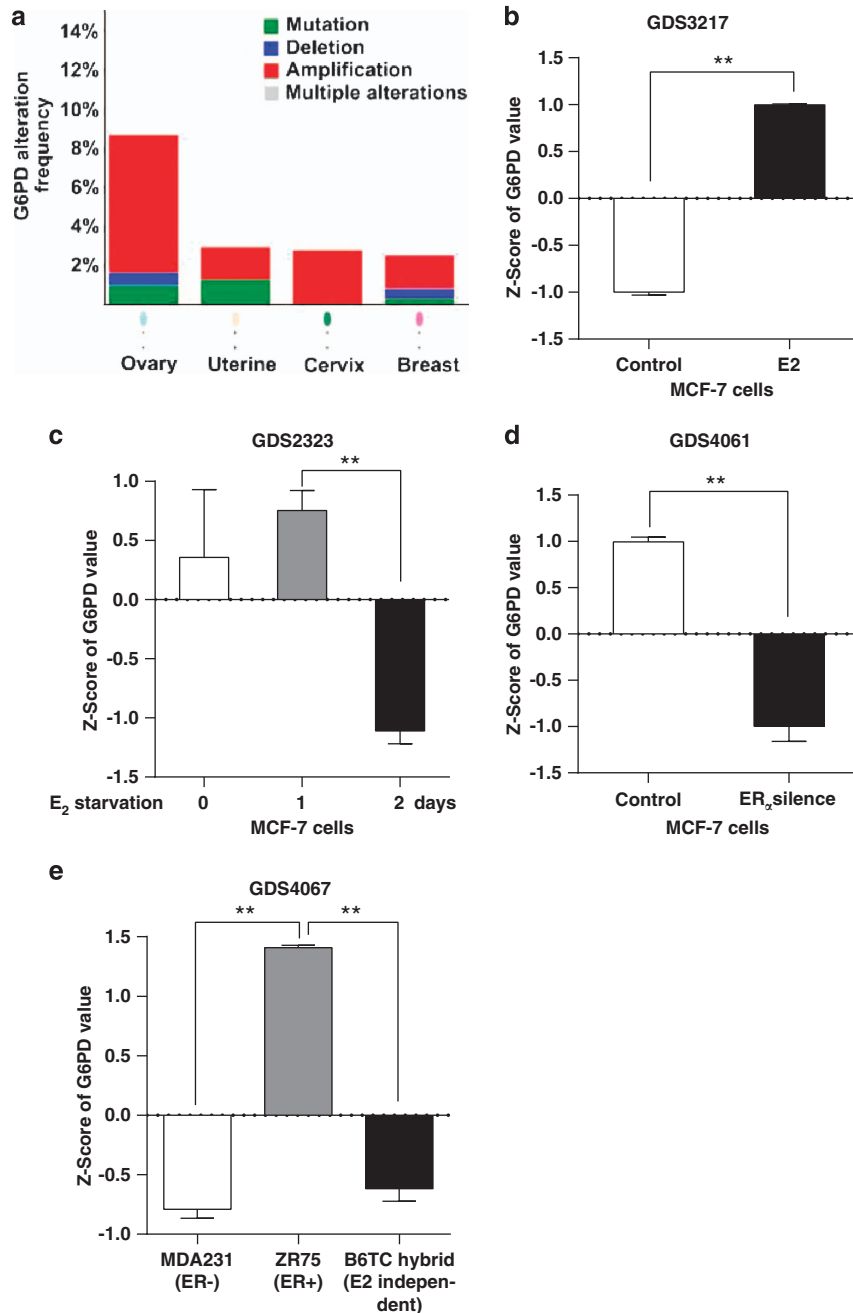


Figure 5 G6PD expression is estradiol-dependent in female cancers. (a) Genomic alterations of *G6pd* were determined in TCGA-curated female cancers including ovary, uterine, cervix, and breast.²³ The colored boxes denote various alterations: green, mutation; dark blue, deletion; red, amplification; gray, multiple alterations. (b–e) Levels of *G6pd* mRNA were determined using cDNA microarray analyses of publicly available microarray data sets. (b) Breast cancer MCF-7 cells were treated with estradiol or control (GEO data set GDS3217). (c) MCF-7 cells were estradiol starved for 0, 1, or 2 days (GEO data set GDS2323). (d) MCF-7 cells were transfected with estrogen receptor α (ER α)-siRNA (ER α silence) or control-siRNA (control) (GEO data set GDS4061). (e) MDA231 (ER-negative), ZR75 (ER-positive), and B6TC hybrid (estrogen-independent) (GEO data set GDS4067). ***P* < 0.01

placebo-treated mice ($P=0.015$, Figure 3i). These data indicate that E_2 enhances glucose uptake by Tsc2-deficient tumor cells *in vivo*.

Estradiol increases the expression of glucose-6-phosphate dehydrogenase *in vitro* and *in vivo*. To explore the impact of E_2 on the flux of glucose to pentose phosphate pathway at the mechanistic level in TSC2-deficient cells, we first examined the transcript levels of glucose-6-phosphate dehydrogenase (G6PD), the first rate-limiting enzyme of the pentose phosphate pathway. E_2 treatment increased the transcript levels of G6PD at 24 h by ~twofold relative to vehicle control in patient-derived cells ($P<0.05$, Figure 4a). It has been reported that G6PD alternative splicing is one of the regulatory mechanisms responsible for G6PD expression.^{21,22} We performed real-time RT-PCR analysis using primers specific to the pre-mRNA and mature mRNA of G6PD. We found that estradiol treatment did not alter the G6PD mature mRNA/pre-mRNA ratio in LAM patient-derived cells (Supplementary Figure S1). Furthermore, cells stimulated by E_2 exhibited higher levels of G6PD protein by ~twofold at 2–24 h in patient-derived cells ($P<0.01$, Figure 4b). Importantly, the estrogen receptor antagonist ICI 182 780 (Faslodex or Fulvestrant) strongly reduced E_2 -increased G6PD protein in patient-derived cells (Figure 4c). To examine whether Akt is a critical mediator of G6PD expression, we treated patient-derived cells with MK-2206 (an allosteric Akt inhibitor), or wortmannin (an irreversible PI3K inhibitor) for 24 h. We found that both inhibitors markedly reduced E_2 -increased G6PD protein (Figure 4c), further supporting that Akt is a critical component in E_2 -altered glucose metabolism in cells lacking TSC2. Interestingly, MEK/1/2 inhibitors AZD6244 or PD98059 had modest effect on E_2 -enhanced G6PD expression (Figure 4c). We also found that E_2 increased the levels of G6PD protein in rat-derived cells within 24 h (Figure 4d), consistent with the findings in patient-derived cells. Importantly, E_2 treatment did not affect the levels of G6PD protein in TSC2-re-expressing patient-derived (Supplementary Figure S2A) or rat-derived cells (Supplementary Figure S2B).

Next, we examined the effect of E_2 on G6PD expression in cells lacking TSC2 *in vivo*. Xenograft tumors of ELT3 cells from E_2 -treated mice exhibited a 3.5-fold increase of G6PD expression relative to placebo treatment ($P<0.01$, Figure 4e).

Immunohistochemistry showed that G6PD accumulation was more evident in xenograft tumors from E_2 -treated mice compared with placebo-treated mice (Figure 4f). Importantly, cells in lung metastatic lesions from E_2 -treated mice showed abundant accumulation of G6PD (Figure 4f). These data demonstrate that E_2 enhances the expression of G6PD in cells lacking TSC2 both *in vitro* and *in vivo*.

G6PD expression is estradiol dependent in female cancers. We have found that estradiol increased the expression of G6PD in mTORC1 hyperactive cells. To examine the levels of G6PD in other female cancers, we first analyzed the frequency of genomic alterations of *G6pd* from The Cancer Genome Atlas (TCGA) data set.²³ Despite the mutation, deletion, and multiple alterations, *G6pd* amplification frequency was higher in ovary cancer (~9%), cervix cancer (3%), uterine cancer (2%), and breast cancer (2%) (Figure 5a). To examine the impact of E_2 on the levels of *G6pd* transcript in breast cancer cells, we analyzed publicly available expression array data sets. E_2 stimulation significantly increased the transcript levels of *G6pd* compared with vehicle control in MCF-7 cells (GDS3217 data set)²⁴ (Figure 5b). E_2 starvation for 2 days significantly decreased the transcript levels of *G6pd* relative to 1-day E_2 starvation or regular condition in MCF-7 cells (GDS2323 data set)²⁵ (Figure 5c). Molecular depletion of ER α reduced the transcript levels of *G6pd* in MCF-7 cells (GDS4061 data set)²⁶ (Figure 5d). Furthermore, ER-positive breast cancer cell line ZR75 displayed higher transcript levels of *G6pd* relative to ER-negative MDA231 cell line and E_2 -independent B6TC hybrid cell line (GDS4067 data set)²⁷ (Figure 5e). Taken together, these data indicate that levels of G6PD are dependent on E_2 and its cognate receptor in female predominant cancers including breast cancer cells, consistent with our findings in TSC2-deficient cells.

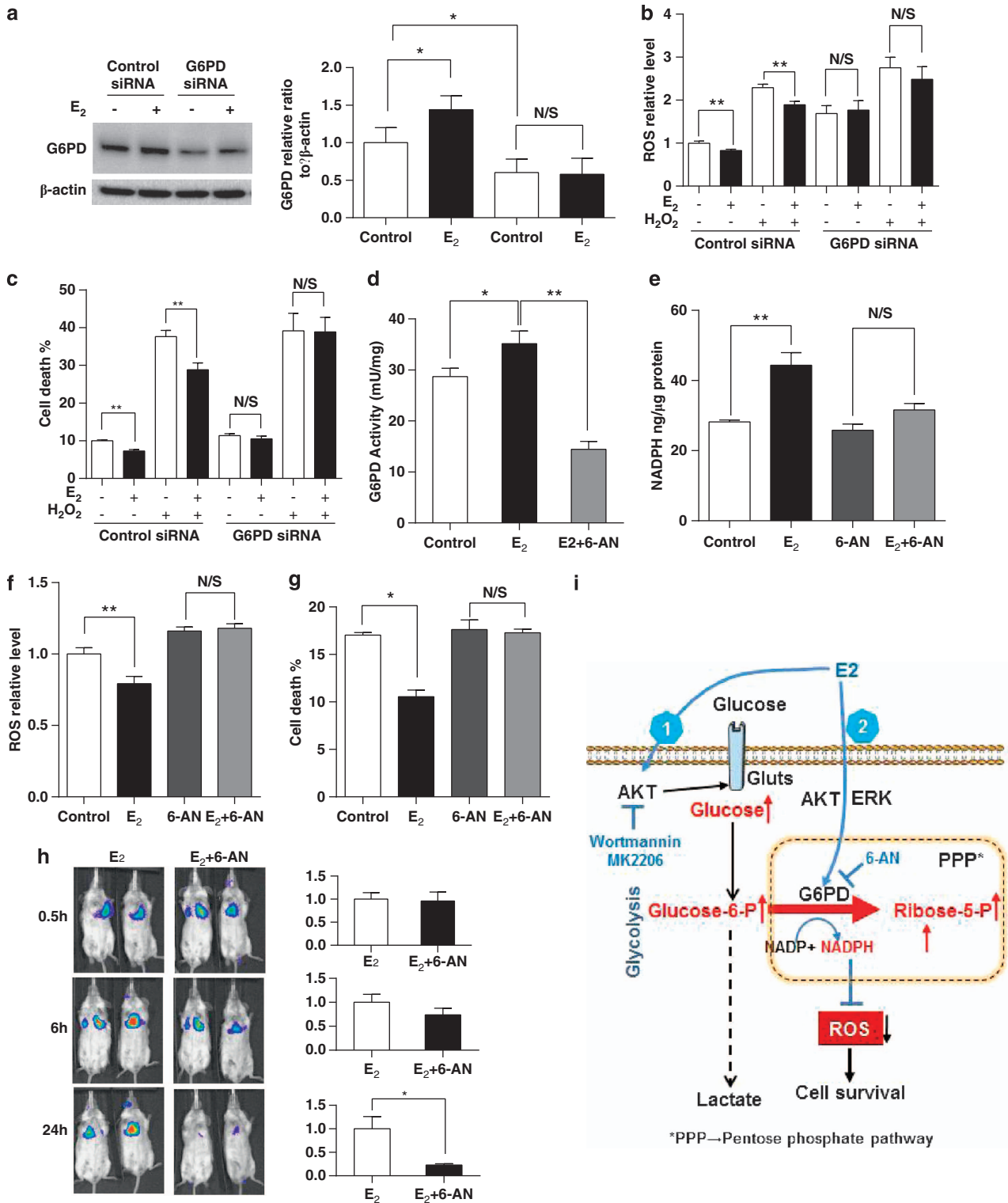
Depletion of G6PD attenuates estradiol-enhanced survival of TSC2-deficient cells *in vitro* and *in vivo*. To determine whether inhibition of G6PD impacts the survival of ELT3 cells *in vitro*, we downregulated G6PD using siRNA in ELT3 cells, achieving ~50% downregulation (Figure 6a). G6PD knockdown prevented E_2 -decreased ROS production in comparison with control siRNA (Figure 6b). Importantly, G6PD downregulation significantly suppressed E_2 -enhanced

Figure 6 Depletion of G6PD attenuates estradiol-enhanced survival of Tsc2-deficient cells *in vitro* and *in vivo*. (a) Tsc2-deficient cells were transfected with control siRNA or G6PD siRNA for 48 h, and then treated with control or estradiol for 6 h. Levels of G6PD, phospho-S6 (Ser235/236), and β -actin were assessed by immunoblot. The graph indicates the ratio of G6PD to β -actin. Results are representative of three different experiments. (b) Tsc2-deficient cells were transfected with control siRNA or G6PD siRNA for 48 h, and then treated with control or estradiol for 24 h. Hydrogen peroxide (0.5 μ M) was added for 1 h before measurement. Cellular ROS level was measured with the DCFH-DA. Data were normalized to total cell number. Results are representative of eight sets of independent samples per group from three experiments. (c) Cell death was measured using propidium iodide (PI) exclusion assay. Data were normalized to total cell number. Results are representative of eight sets of independent samples per group from three experiments. (d) Tsc2-deficient cells were treated with 6-AN (10 μ M) for 1 h, and then treated with control or estradiol for 24 h. G6PD activity was determined. (e) Tsc2-deficient cells were treated with 6-AN (10 μ M) for 1 h, and then treated with control or estradiol (10 nM) for 2 and 24 h. Cellular NADPH level was measured. Data were normalized to total protein level. Results are representative of three sets of independent samples per group from three experiments. (f) Tsc2-deficient cells were treated with 6-AN (10 μ M) for 1 h, and then treated with control or estradiol (10 nM) for 24 h. Cellular ROS level was measured with the DCFH-DA. Data were normalized to cell number. Results are representative of eight sets of independent samples per group from three experiments. (g) Tsc2-deficient cells were treated with 6-AN (10 μ M) for 1 h, and then treated with control or estradiol (10 nM) for 24 h. Cell death was measured using the PI exclusion assay. Data were normalized to cell number. Results are representative of eight sets of independent samples per group from three experiments. (h) Female CB17 SCID mice were supplemented with estradiol for 1 week, and then treated with 6-AN or vehicle for 2 days. ELT3-luciferase cells were treated with 6-AN for 18 h, and then injected intravenously into mice ($n=5$ /group). Lung colonization was measured using bioluminescence at 0.5, 6, and 24 h after injection. Representative images are shown. Total photon flux/second present in the chest regions in estradiol ($n=5$) and estradiol plus 6-AN-treated ($n=5$) animals. (i) Scheme of estradiol-promoted pentose phosphate pathway addition in TSC2-deficient cells. * $P<0.05$, ** $P<0.01$

survival of Tsc2-deficient ELT3 cells after H₂O₂ treatment (Figure 6c).

To inhibit G6PD pharmacologically, we treated Tsc2-deficient cells with 6-AN, an inhibitor of G6PD and pentose phosphate pathway. 6-AN treatment significantly decreased

E₂-induced G6PD activity ($P < 0.01$, Figure 6d), E₂-enhanced cellular level of NADPH ($P < 0.01$, Figure 6e), and E₂-reduced ROS production ($P < 0.05$, Figure 6f). Importantly, 6-AN treatment significantly suppressed E₂-enhanced survival of ELT3 cells after H₂O₂ treatment ($P < 0.05$, Figure 6g).



These data indicate that depletion of G6PD attenuates E₂-enhanced survival of ELT3 cells *in vitro*.

To investigate further the role of G6PD on the survival of ELT3 cells *in vivo*, ELT3 luciferase cells²⁸ were intravenously injected into mice treated with E₂ alone or E₂ plus 6-AN. At 0.5 and 6 h post cell inoculation, similar levels of bioluminescence were observed in the chest regions of all mice. At 24 h, the bioluminescence in the chest regions of the E₂ plus 6-AN-treated mice was decreased by ~80% as compared with that in the E₂-treated mice ($P < 0.05$, Figure 6h). These data support a model in which inhibition of G6PD attenuates E₂-enhanced survival of Tsc2-deficient cells *in vivo*.

Discussion

LAM is a female predominant lung disease characterized by the abnormal proliferation of smooth muscle cells and progressive cyst formation that can lead to respiratory failure.^{1–3} The gender specificity of LAM suggests that estradiol may contribute to disease progression, whereas mTORC1, which is hyperactive in LAM cells, is a master regulator of cellular metabolism. However, the role of estradiol in regulating the metabolism in Tsc2-deficient cells has not been extensively investigated. In this study, we identified an estradiol-enhanced glucose and pentose phosphate pathway signature in Tsc2-deficient rat uterine leiomyoma-derived ELT3 cells *in vitro*. Estradiol treatment led to increased cellular NADPH and decreased ROS and enhanced cell survival under oxidative stress. Estradiol also induced plasma membrane translocation of GLUT1 or GLUT4 and increased glucose uptake in a PI3K/Akt-dependent manner. ¹⁸F-FDG-PET/CT imaging showed enhanced glucose uptake in xenograft tumors from estradiol-treated mice. Depletion of G6PD, a rate-limiting enzyme for the pentose phosphate pathway, suppressed estradiol-enhanced survival of Tsc2-deficient cells *in vitro* and *in vivo*. Collectively, these data indicate that estradiol promotes glucose metabolism through the pentose phosphate pathway in cells with mTORC1 hyperactivation and enhances cell survival under oxidative stress.

Alterations in cellular energy metabolism are a hallmark of cancer,⁶ and there are many indications that metabolic reprogramming is particularly critical for the survival of Tsc2-deficient cells. Glucose addiction of Tsc2-deficient cells has been reported,⁸ suggesting that glucose metabolism is essential for the survival of Tsc2-deficient cells. TSC2 deficiency leads to increased transcript levels of glucose metabolism genes.¹⁰ Cells with mTORC1 activation express high levels of glycolytic proteins PKM2.¹¹ Somewhat surprisingly, however, the mTORC1 inhibitor rapamycin reduces lactate production but does not affect cellular ATP levels in *Tsc2*^{-/-} MEF cells.⁹ Together, these reports highlight connections between cellular metabolic alterations and glucose utilization that is likely to impact TSC2-deficient LAM cells.

¹⁸F-FDG-PET scanning has been performed in LAM patients. One case report described a strong FDG uptake in pulmonary LAM.²⁹ Moreover, Young *et al.*³⁰ performed FDG-PET scanning in 12 LAM patients and FDG-PET was negative for all patients. Reasons for the negativity of FDG-PET in LAM patients may include: (1) the sensitivity of PET detection because of the diffused infiltration of LAM

cells; (2) emphysema-like destruction of lung parenchyma;¹ (3) downregulation and cytoplasmic localization of glucose transporters in cells lacking TSC2;³¹ (4) glucose uptake and PET positivity may be cyclical, depending on circulating estrogen levels.

We previously showed that estradiol promotes the metastasis of Tsc2-deficient ELT3 tumors in a MEK1/2-dependent manner.²⁸ Here, we report that estradiol promotes glucose metabolism via the pentose phosphate pathway in TSC2-deficient cells, associated with a MEK1/2-independent but PI3K/Akt-dependent plasma membrane translocation of GLUT1 or GLUT4. This is particularly interesting, because it has been previously demonstrated that GLUT1 and GLUT4 are localized in the cytoplasm but not in the plasma membrane in Tsc2-deficient cells,³¹ which may limit their ability to proliferate especially under conditions of bioenergetic stress. Our finding that estradiol is sufficient to restore membrane localization of the GLUT1 or GLUT4 transporter and enhance glucose uptake may, therefore, represent a key pathogenic mechanism underlying the female predominance of LAM (Figure 6i).

LAM can lead to respiratory failure and death.^{1–3} The recent MILES trial demonstrated that the mTORC1 inhibitor Sirolimus stabilizes lung function in women with LAM. However, lung function decline resumed upon drug discontinuation.³² Therefore, despite many advances in the clinical care of women with LAM, there remains a critical need for improved therapeutic options. The fact that estradiol promotes glucose utilization and cell survival via the pentose phosphate pathway suggests that inhibiting the PPP could selectively inhibit estrogen-induced cell survival. Consistent with this hypothesis, we found that 6-AN blocked estrogen-induced survival both *in vivo* and *in vitro*, suggesting a novel therapeutic approach for LAM. Our data suggest that inhibiting estrogen-dependent cellular metabolic pathways could block the pro-survival effects of estrogen on LAM cells, without the need to ablate the entire hormonal signaling axis. In the long term, it is possible that metabolically focused strategies in LAM could have preferable side effect profiles compared with hormonal ablation in terms of bone health and other parameters; clearly additional pre-clinical and clinical studies will be needed to test this concept.

Materials and Methods

Cell line and culture. Eker rat uterine leiomyoma-derived cells (ELT3),^{14,15} ELT3 luciferase-expressing cells,²⁸ and LAM patient-derived cells (developed from a sporadic LAM-associated renal angiomyolipoma cells carrying biallelic mutations of the *TSC2* gene³³) were cultured in IIA complete medium supplemented with 10% FBS. Prior to estradiol stimulation, cells were starved in serum-free and phenol red-free IIA media for 24 h.

Antibodies and chemicals. The following chemicals were used: 17-beta-estradiol, wortmannin and DAPI (Sigma-Aldrich, St. Louis, MO, USA), rapamycin (L C Laboratories, Woburn, MA, USA), PD98059 (Cell Signaling Technologies, Danvers, MA, USA), MK2206 (Active Biochem, Maplewood, NJ, USA), and AZD6244 (L C Laboratories). Antibodies included phospho-ERK1/2 (T202/Y204), phospho-S6 (S235/236), phospho-Akt (S473) and TSC2 (Cell Signaling Technologies), G6PD and GLUT1 (H-43) (Santa Cruz Biotechnology, Dallas, TX, USA), GLUT4 and β -actin (Sigma-Aldrich), and Alexa Fluor 488 Goat Anti-Rabbit IgG (Invitrogen, Grand Island, NY, USA).

Metabolomic profiling. Cell pellets were submitted to Metabolon Inc. (Durham, NC, USA) for sample extraction and analysis. Briefly, Metabolon

performed cold methanol extraction of cell pellets and these extracts were split into three aliquots. These aliquots were processed and characterized by one of the three analytical methods previously described.^{34,35}

Cellular NADPH quantification. Cells were seeded in 12-well plates, treated with siRNA or inhibitors, and then stimulated with control or estradiol (10 nM). Cells (1×10^5) were harvested and lysates were extracted with 200 μ l of extraction buffer following the manufacture's instruction. Levels of NADPH were measured using the NADP/NADPH Assay kit (Abcam, Cambridge, MA, USA) and normalized to total cellular proteins.

Quantification of ROS. Cells were seeded in 96-well plates and incubated with 50 μ M DCFH-DA in $1 \times$ -DPBS for 45 min at 37 °C. Fluorescence was read at 485 nm/525 nm. Levels of cellular ROS were normalized to the total number of cells.

Measurement of cell survival. Cells were plated in 96-well plates, incubated with propidium iodide (5 μ M) in 100 μ l $1 \times$ -DPBS for 30 min at 37 °C. Fluorescence was read at 530 nm/620 nm. Data were represented as percentage of dead cells relative to the total number of cells. Cell growth was measured using crystal violet assay.

Immunoblotting. Cells were lysed in M-PER buffer (Pierce, Rockford, IL, USA) supplemented with protease inhibitors and phosphatase inhibitor cocktails. Cleared cell lysates were obtained by centrifugation at 14 000 r.p.m. for 10 min at 4 °C and then subjected to immunoblotting.

Animal studies. All animal work was performed in accordance with protocols approved by the Institutional Animal Care and Use Committee-Children Hospital Boston. For xenograft tumor establishment, 1 week before cell inoculation, mice were implanted with estradiol pellets (90-day release, 2.5 mg/pellet, Innovative Research of America, Sarasota, FL, USA) or placebo pellets. Two million ELT3 cells were inoculated bilaterally into the posterior back region of the mice. Mice bearing subcutaneous tumors (\sim 250 mm³) underwent FDG-PET scanning. For the intravenous model, 0.5 million ELT3 luciferase cells in a volume of 100 μ l were injected intravenously into the tail vein of the CB-17 SCID mice pretreated with estradiol (500 nM in drinking water) for 2 days before cell injection.

Immunohistochemistry. Sections were deparaffinized, incubated with primary antibodies and biotinylated secondary antibodies, and counterstained with Gill's Hematoxylin.

Immunofluorescence. Cells were plated on glass coverslips, serum starved overnight, treated with rapamycin (10 nM) or wortmannin (500 nM) for 15 min, and then stimulated with control or estradiol (10 nM) for 12 or 24 h. Cells were fixed with 50% methanol plus 50% acetone for 2 min, blocked in 1% BSA/PBS/Tween 20 (0.05%) for 30 min, incubated with primary antibody for 1 h and then secondary antibodies for 1 h. Images were captured with a FluoView FV-10i Olympus Laser Point Scanning Confocal Microscope, Olympus (Center Valley, PA, USA).

2-NBDG uptake. 2-[N-(7-nitrobenz-2-oxa-1,3-diazol-4-yl)amino]-2-deoxyglucose (2-NBDG, Cayman Chemical, Ann Arbor, MI, USA), a glucose analog fluorescently labeled at the two position, is a substrate for glucose transporters.³⁶ Cells were cultured in IIA medium with 10% FBS, starved with serum-free and phenol-free IIA medium overnight, pretreated with inhibitors for 15 min, and then stimulated with E₂ (10 nM) for 24 h. Medium was changed to phenol-free serum-free glucose-free DMEM with 50 μ mol/l 2-NBDG for 30 min. Internalization of 2-NBDG was monitored using confocal microscopy. 2-NBDG uptake was quantified using fluorescence intensity and normalized to control.

Glucose assay. Cells were seeded in 12-well plates, treated with inhibitors, and then stimulated with control or estradiol (10 nM). Conditioned media was collected and subjected to glucose quantification using the Glucose (HK) Assay Kit (Sigma-Aldrich).

¹⁸F-FDG-PET imaging. Mice bearing subcutaneous tumors (\sim 250 mm³) were intravenously injected with 150 μ Ci of [¹⁸F]FDG. After 30 min, animals were anesthetized with 2% isoflurane, and imaged for 15 min using a small animal

PET/CT scanner (eXplore Vista, GE Healthcare, Waukesha, WI, USA). Images were reconstructed using Fourier rebinning (FORE) and ordered subsets expectation maximization algorithm with 16 subsets and 2 iterations. The voxel dimensions of the reconstructed images were $0.39 \times 0.39 \times 0.78$ mm³. [¹⁸F]FDG uptake in each mouse normalized to the body weight and injected FDG dose, and was presented as SUV.

TCGA data analysis. Genomic alterations of *G6pd* data for all TCGA cases were analyzed from TCGA data sets obtained from the cBioPortal for Cancer Genomics (<http://www.cbioportal.org/public-portal/index.do>).

Gene expression analysis. The publicly available microarray GEO data sets (www.ncbi.nlm.nih.gov/geo/) were collected. The Z-score of *G6pd* mRNA was used for data analysis.

siRNA transfection. Control-siRNA (50 nM) or *G6PD*-siRNA (Dharmacon, Pittsburgh, PA, USA) were transfected in cells using TransIT-TKO reagent (Mirus, Madison, WI, USA). Cells were harvested at 48–60 h post transfection.

G6PD activity assay. Cells were seeded in 12-well plates, treated with inhibitors, and then stimulated with control or estradiol (10 nM). Cells (1×10^5) were collected and lysates were extracted with 200 μ l of extraction buffer following the manufacture's protocol. *G6PD* activity was quantified using *G6PD* Activity Colorimetric Assay kit (Biovision, Milpitas, CA, USA). *G6PD* activity was normalized to total protein levels.

Bioluminescent reporter imaging. Ten minutes before imaging, animals were injected with luciferin (Xenogen, Waltham, MA, USA) (120 mg/kg, i.p.). Bioluminescent signals were recorded using the Xenogen IVIS System. Total photon flux of the chest area was analyzed.²⁸

Statistical analyses. All data are shown as mean \pm S.E.M. Measurements at single time points were analyzed by ANOVA and, if they demonstrated significance, were further analyzed by a two-tailed *t*-test. All statistical tests were conducted using GraphPad Prism 6.0 (GraphPad Software, San Diego, CA, USA). *P* < 0.05 was used to define statistical significance.

Conflict of Interest

The authors declare no conflict of interest.

Acknowledgements. We are grateful for Dr. C Walker (Texas A&M Health Science Center) for providing ELT3 cells. This study is supported by The LAM Foundation, The Adler Foundation, The LAM Treatment Alliance, the National Institute of Diabetes and Digestive and Kidney Diseases, and the National Heart Lung and Blood Institute to EPH, The LAM Foundation grant and NIH Grant GM51405 to JB, and the National Heart Lung and Blood Institute (HL98216) to JJY. XG is a LAM Foundation fellow.

1. Henske EP, McCormack FX. Lymphangioleiomyomatosis—a wolf in sheep's clothing. *J Clin Invest* 2012; **122**: 3807–3816.
2. McCormack FX, Travis WD, Colby TV, Henske EP, Moss J. Lymphangioleiomyomatosis: calling it what it is: a low-grade, destructive, metastasizing neoplasm. *Am J Respir Crit Care Med* 2012; **186**: 1210–1212.
3. Moss J. Focus on lymphangioleiomyomatosis. introduction. *Lymphatic Res Biol* 2010; **8**: 3.
4. Carsillo T, Astrinidis A, Henske EP. Mutations in the tuberous sclerosis complex gene *TSC2* are a cause of sporadic pulmonary lymphangioleiomyomatosis. *Proc Natl Acad Sci USA* 2000; **97**: 6085–6090.
5. Karbowniczek M, Astrinidis A, Balsara BR, Testa JR, Lium JH, Colby TV *et al*. Recurrent lymphangioleiomyomatosis after transplantation: genetic analyses reveal a metastatic mechanism. *Am J Respir Crit Care Med* 2003; **167**: 976–982.
6. Hanahan D, Weinberg RA. Hallmarks of cancer: the next generation. *Cell* 2011; **144**: 646–674.
7. Warburg O. On the origin of cancer cells. *Science* 1956; **123**: 309–314.
8. Inoki K, Zhu T, Guan KL. *TSC2* mediates cellular energy response to control cell growth and survival. *Cell* 2003; **115**: 577–590.
9. Choo AY, Kim SG, Vander Heiden MG, Mahoney SJ, Vu H, Yoon SO *et al*. Glucose addiction of *TSC* null cells is caused by failed mTORC1-dependent balancing of metabolic demand with supply. *Mol Cell* 2010; **38**: 487–499.

10. Duvel K, Yecies JL, Menon S, Raman P, Lipovsky AI, Souza AL *et al*. Activation of a metabolic gene regulatory network downstream of mTOR complex 1. *Mol Cell* 2010; **39**: 171–183.
11. Sun Q, Chen X, Ma J, Peng H, Wang F, Zha X *et al*. Mammalian target of rapamycin up-regulation of pyruvate kinase isoenzyme type M2 is critical for aerobic glycolysis and tumor growth. *Proc Natl Acad Sci USA* 2011; **108**: 4129–4134.
12. Parkhitko AA, Priolo C, Coloff JL, Yun J, Wu JJ, Mizumura K *et al*. Autophagy-dependent metabolic reprogramming sensitizes TSC2-deficient cells to the antimetabolite 6-aminocaproic acid. *Mol Cancer Res MCR* 2014; **12**: 48–57.
13. Polimeni M, Voena C, Kopecka J, Riganti C, Pescarmona G, Bosia A *et al*. Modulation of doxorubicin resistance by the glucose-6-phosphate dehydrogenase activity. *Biochem J* 2011; **439**: 141–149.
14. Howe SR, Gottardis MM, Everitt JI, Walker C. Rodent model of reproductive tract leiomyomata. Establishment and characterization of tumor-derived cell lines. *Am J Pathol* 1995; **146**: 1568–1579.
15. Howe SR, Gottardis MM, Everitt JI, Walker C. Estrogen stimulation and tamoxifen inhibition of leiomyoma cell growth in vitro and in vivo. *Endocrinology* 1995; **136**: 4996–5003.
16. Gu X, Yu JJ, Ilter D, Blenis N, Henske EP, Blenis J. Integration of mTOR and estrogen-ERK2 signaling in lymphangiogenesis pathogenesis. *Proc Natl Acad Sci USA* 2013; **110**: 14960–14965.
17. Finlay GA, Hunter DS, Walker CL, Paulson KE, Fanburg BL. Regulation of PDGF production and ERK activation by estrogen is associated with TSC2 gene expression. *Am J Physiol Cell Physiol* 2003; **285**: C409–C418.
18. Finlay GA, York B, Karas RH, Fanburg BL, Zhang H, Kwiatkowski DJ *et al*. Estrogen-induced smooth muscle cell growth is regulated by tuberin and associated with altered activation of platelet-derived growth factor receptor-beta and ERK-1/2. *J Biol Chem* 2004; **279**: 23114–23122.
19. Manning BD, Logsdon MN, Lipovsky AI, Abbott D, Kwiatkowski DJ, Cantley LC. Feedback inhibition of Akt signaling limits the growth of tumors lacking Tsc2. *Genes Dev* 2005; **19**: 1773–1778.
20. Faulds MH, Zhao C, Dahlman-Wright K, Gustafsson JA. The diversity of sex steroid action: regulation of metabolism by estrogen signaling. *J Endocrinol* 2012; **212**: 3–12.
21. Tao H, Szeszel-Fedorowicz W, Amir-Ahmady B, Gibson MA, Stabile LP, Salati LM. Inhibition of the splicing of glucose-6-phosphate dehydrogenase precursor mRNA by polyunsaturated fatty acids. *J Biol Chem* 2002; **277**: 31270–31278.
22. Hong X, Song R, Song H, Zheng T, Wang J, Liang Y *et al*. PTEN antagonizes Tc11/hnRNP-mediated G6PD pre-mRNA splicing which contributes to hepatocarcinogenesis. *Gut* 2013; e-pub ahead of print 18 December 2013; doi:10.1136/gutjnl-2013-305302.
23. Hanauer DA, Rhodes DR, Sinha-Kumar C, Chinnaiyan AM. Bioinformatics approaches in the study of cancer. *Curr Mol Med* 2007; **7**: 133–141.
24. Lin CY, Vega VB, Thomsen JS, Zhang T, Kong SL, Xie M *et al*. Whole-genome cartography of estrogen receptor alpha binding sites. *PLoS Genet* 2007; **3**: e87.
25. Coser KR, Chesnes J, Hur J, Ray S, Isselbacher KJ, Shioda T. Global analysis of ligand sensitivity of estrogen inducible and suppressible genes in MCF7/BUS breast cancer cells by DNA microarray. *Proc Natl Acad Sci USA* 2003; **100**: 13994–13999.
26. Al Saleh S, Al Mulla F, Luqmani YA. Estrogen receptor silencing induces epithelial to mesenchymal transition in human breast cancer cells. *PLoS One* 2011; **6**: e20610.
27. Mukhopadhyay KD, Bandyopadhyay A, Chang TT, Elkahoul AG, Cornell JE, Yang J *et al*. Isolation and characterization of a metastatic hybrid cell line generated by ER negative and ER positive breast cancer cells in mouse bone marrow. *PLoS One* 2011; **6**: e20473.
28. Yu JJ, Robb VA, Morrison TA, Ariazi EA, Karbowiczek M, Astrinidis A *et al*. Estrogen promotes the survival and pulmonary metastasis of tuberin-null cells. *Proc Natl Acad Sci USA* 2009; **106**: 2635–2640.
29. Pandit N, Yeung HW. F-18 FDG uptake in pulmonary lymphangiomyomatosis. *Clin Nuclear Med* 2001; **26**: 1050–1051.
30. Young LR, Franz DN, Nagarkatte P, Fletcher CD, Wikenheiser-Brookamp KA, Galsky MD *et al*. Utility of [18F]2-fluoro-2-deoxyglucose-PET in sporadic and tuberous sclerosis-associated lymphangiomyomatosis. *Chest* 2009; **136**: 926–933.
31. Jiang X, Kenerson H, Aicher L, Miyaoka R, Eary J, Bissler J *et al*. The tuberous sclerosis complex regulates trafficking of glucose transporters and glucose uptake. *Am J Pathol* 2008; **172**: 1748–1756.
32. McCormack FX, Inoue Y, Moss J, Singer LG, Strange C, Nakata K *et al*. Efficacy and safety of sirolimus in lymphangiomyomatosis. *N Engl J Med* 2011; **364**: 1595–1606.
33. Yu J, Astrinidis A, Howard S, Henske EP. Estradiol and tamoxifen stimulate LAM-associated angiomyolipoma cell growth and activate both genomic and nongenomic signaling pathways. *Am J Physiol Lung Cell Mol Physiol* 2004; **286**: L694–L700.
34. Evans AM, DeHaven CD, Barrett T, Mitchell M, Milgram E. Integrated, nontargeted ultrahigh performance liquid chromatography/electrospray ionization tandem mass spectrometry platform for the identification and relative quantification of the small-molecule complement of biological systems. *Anal Chem* 2009; **81**: 6656–6667.
35. DeHaven CD, Evans AM, Dai H, Lawton KA. Organization of GC/MS and LC/MS metabolomics data into chemical libraries. *J Cheminform* 2010; **2**: 9.
36. O'Neil RG, Wu L, Mullani N. Uptake of a fluorescent deoxyglucose analog (2-NBDG) in tumor cells. *Mol Imaging Biol* 2005; **7**: 388–392.



Cell Death and Disease is an open-access journal published by Nature Publishing Group. This work is licensed under a Creative Commons Attribution-NonCommercial-NoDerivs 3.0 Unported License. The images or other third party material in this article are included in the article's Creative Commons license, unless indicated otherwise in the credit line; if the material is not included under the Creative Commons license, users will need to obtain permission from the license holder to reproduce the material. To view a copy of this license, visit <http://creativecommons.org/licenses/by-nc-nd/3.0/>

Supplementary Information accompanies this paper on Cell Death and Disease website (<http://www.nature.com/cddis>)